Crystal Structure of $Nd_2BaCu_3O_{7.3}$ Determined from X-ray and Neutron Powder Diffraction Data

V. V. Petrykin,*,† P. Berastegui,‡ and M. Kakihana†

Materials and Structures Laboratory, Tokyo Institute of Technology, 4259 Nagatsuta, Midori, Yokohama 226-8503, Japan, and Department of Inorganic Chemistry, Chalmers University of Technology and University of Göteborg, S41296 Göteborg, Sweden

Received January 11, 1999. Revised Manuscript Received October 8, 1999

In the present paper we report crystal structure of insulating compound $Nd_{1.9}Ba_{1.1}Cu_3O_{7.28}$—the Nd-rich terminating point of $Nd_{1+x}Ba_{2-x}Cu_3O_z$ solid solutions. This phase has an orthorhombic lattice with $a = 3.8565(1)$ Å, $b = 7.7724(3)$ Å, $c = 22.9862(8)$ Å. The space group *Ammm* was determined on the basis of IR and Raman spectroscopic data and electron diffraction analysis. The crystal structure was solved and refined from the powder XRD and time-of-flight neutron diffraction data. Neodymium atoms on the barium site compared to conventional $NdBa_2Cu_3O_7$ crystal are ordered and form a face-centered supercell, while additional oxygen atoms occupy vacant chain sites in the vicinity of barium atoms.

Introduction

The phase diagram in the system Nd_2O_3−BaO−CuO was studied by several groups[1−7] since the discovery of high-temperature superconductivity in cuprates. The maximum substitution of Nd for Ba in the solid solutions with general formula of $Nd_{1+x}Ba_{2-x}Cu_3O_z$ is reported to be between $x = 0.7$ and $x = 1.0$, depending on $P_{O_2} - T$ conditions.[3,5]

The crystal structures of $Nd_{1+x}Ba_{2-x}Cu_3O_z$ solid solutions with x up to 0.5 were investigated using powder X-ray diffraction,[8] neutron diffraction,[9−11] and X-ray data collected on single crystals.[12] It was established that solid solutions have a crystal structure similar to $NdBa_2Cu_3O_7$ phase in which Ba atoms can be substituted by Nd and additional oxygen atoms occupy normally vacant sites between Cu−O chains. The disorder introduced by substitution and incorporation of extra oxygen atoms results in the decrease of orthorhombicity, and for $x > 0.20$−0.25 only tetragonal phases can be obtained.[1,5,6,8,11] The substitution of Nd onto the Ba site also leads to a reduction in critical temperature and for x values higher than 0.5 superconductivity disappears. This was one of the reasons why solid solutions with high Nd concentration did not attract much attention.

Recently it was found[6] that homogeneous precursors allowed the synthesis of single-phase samples with x as high as 0.9, and the compound had a unit cell with $a = 2a_{123}$, $b = b_{123}$ and $c = 2c_{123}$ supercell. The orthorhombic distortion for $x = 0.9$ is present on the XRD patterns in earlier studies.[4] The latter fact did not attract much attention, and small amount of Nd_2CuO_4 detected in the sample led authors to conclude a smaller solubility limit for Nd in $Nd_{1+x}Ba_{2-x}Cu_3O_z$ solid solution. Recently we found[13] that the crystal structure of the newly reported[6] phase, determined from powder XRD, cannot explain the existence of the significant oxygen nonstoichiometry. The more reliable result of neutron diffraction studies[14] brought an explanation to the variable oxygen content; however, the choice of *B*2*mm* space group[6,14] could not account for the observed Raman spectrum of this compound.[13]

There are several extra modes observed in Raman spectrum of $Nd_2BaCu_3O_{7.3}$ compared to the spectrum of $NdBa_2Cu_3O_7$ compound. These frequencies are close to the vibration frequencies of apical oxygen and oxygen in CuO_2 planes in simple $NdBa_2Cu_3O_7$[15] which does not have the supercell. However, for noncentrosymmetric space group *B*2*mm* proposed previously,[6,14] all possible

† Tokyo Institute of Technology.
‡ Chalmers University of Technology and University of Göteborg.

(1) Wong-Ng, W.; Paretzkin, B.; Edwin, R.; Fuller, Jr. *J Solid State Chem.* **1990**, *85*, 117.
(2) Yoo, S. I.; McCallum, R. W. *Physica C* **1993**, *210*, 147.
(3) Osamura, K.; Zhang, W. Z. *Metallkd.* **1993**, *84*, 522.
(4) Wong-Ng, W.; Cook, L. P.; Paretzkin, B.; Hill, M. D.; Stalick, J. K. *J. Am. Ceram. Soc.* **1994**, *77*, 2354.
(5) Lindemer, T. B.; Specht, E. D.; Martin, P. M.; Flitcroft, M. L. *Physica C* **1995**, *255*, 65.
(6) Goodilin, E. A.; Oleynikov, N. N.; Antipov, E. V.; Shpanchenko, R. V.; Popov, G. Yu.; Balakirev, V. G.; Tretyakov, Yu. D. *Physica C* **1996**, *272*, 65.
(7) Kambara, M.; Umeda, T.; Tagami, M.; Goodilin, E. A.; Shiohara, Y. *J. Am. Ceram. Soc.* **1998**, *81*, 2116.
(8) Takita, K.; Katoh, H.; Akinaga, H.; Nishino, M.; Ishigaki, T.; Asano, H. *Jpn. J. Appl. Phys.* **1988**, *27*, L57.
(9) Izumi, F.; Takekawa, S.; Matsui, Y.; Iyi, N.; Asano, H.; Ishigaki, T.; Watanabe, N. *Jpn. J. Appl. Phys.* **1987**, *26*, L1616.
(10) Ren, Y.; Tang, H. B.; Yan, Q. W.; Zhang, P. L.; Liu, Y. L.; Cui, C. G.; Ning, T. S.; Zhang, Z. *Phys. Rev. B* **1988**, *38*, 11861.
(11) Allenspach, P.; Mesot, J.; Staub, U.; Guillaume, M.; Furrer, A.; Yoo, S.-I.; Kramer, M. J.; McCallum, R. W.; Maletta, H.; Blank, H.; Mutka, H.; Osborn, R.; Arai, M.; Bowden, Z.; Taylor, A. D. *Z. Phys. B* **1994**, *95*, 301.
(12) Fomichev, D. V.; Dyachenko, O. G.; Mironov, A. V.; Antipov, E. V. *Physica C* **1994**, *225*, 25.
(13) Petrykin, V. V.; Goodilin, E. A.; Kakihana, M.; Tretyakov, Yu. D. *Key Eng. Mater.* **1997**, *132*−*136*, 1285.
(14) Goodilin, E.; Khasanova, N.; Wu, X. J.; Kamiyama, T.; Izumi, F.; Tajima, S.; Shiohara Y. In *Proceedings of the NATO Advanced Research Workshop on High-Temperature Superconductors and Novel Inorganic Materials Engineering MSU*−*HTSC V*; Van Tendeloo, G., Antipov, E. V., Putilin, S. N., Eds.; Moscow, Russia, March 24−29, 1998; 145.
(15) Nishitani, R.; Yoshida, N.; Saski, Y.; Nishina, Y. *Jpn. J. Appl. Phys.* **1989**, *28*, L569.

10.1021/cm990021w CCC: $18.00
Published on Web 11/29/1999

vibrations are allowed in both Raman and IR spectra. One could expect at least 36 Raman active modes in this material even if one neglects the possibility of the superstructure.

In the present paper we report the results of our investigation on the "$Nd_2BaCu_3O_{7.3}$" phase by Raman and IR spectroscopies and electron diffraction analysis that helped to determine the correct space group and crystal structure. The structure of new compound was solved and refined using powder XRD and time-of-flight (TOF) neutron diffraction data. Understanding of the Nd−Ba and oxygen atoms arrangement in the $Nd_{1+x}Ba_{2-x}Cu_3O_z$ solid solution is essential for explanation of hole-doping mechanisms and related suppression of superconductivity as well as for the superconducting materials design and fabrication in this system.

Experimental Section

The samples with the nominal composition of $Nd_{1.95}Ba_{1.1}Cu_3O_z$ and $Nd_{1.95}Ba_{1.05}Cu_3O_z$ were prepared by polymerized complex method[16] using stoichiometric amounts of Nd_2O_3 (99.99%), $BaCO_3$ (99.0%), and $CuCO_3{\cdot}Cu(OH)_2$ (CuO content is 67.28 wt %); citric acid (CA), ethylene glycol (EG), and HNO_3 (ρ = 1.38 g cm^{-3}) reagent-grade quality were obtained from commercial sources. Neodymium oxide was preliminary heated at 950 °C and then dissolved in 20% excess of HNO_3. Citric acid (CA) and ethylene glycol (EG) were added to this solution and stirred at 80 °C until complete dissolution. Stoichiometric amounts of $BaCO_3$ and $Cu_2(OH)_2CO_3$ were dissolved in this solution. The temperature was raised to 140 °C and kept constant for 4 h until a dark-green gel formed. Finally, the temperature was increased up to 200 °C for evaporation of excess of EG. Molar ratio of cation/CA/EG was 1/5/20. The powder obtained after calcination of brown polymer at 450 °C for 5 h was annealed in air at 900 °C for 15 h. The powder was then ground, pressed into pellets, and sintered at 980 °C in flowing oxygen for 48 h with the subsequent quenching into liquid nitrogen. Finally, the samples were annealed in oxygen at 400 °C for 60 h. Oxygen content of the prepared solid solutions was determined by iodometric titration.

The X-ray diffraction patterns were collected by a MacScience diffractometer equipped with a diffracted beam graphite monochromator using Cu Ka radiation in Bragg−Brentano configuration. Lattice constants were calculated by the least-squares method with Si as internal standard using relatively fast scanning speed (step size, 0.02; acquisition time, 5 s/step). For structural analysis we used the XRD pattern recorded in the scanning-step mode with the step size 0.01 deg and 8 s/step. To solve and refine crystal structure GSAS[17] and SHELXS[18] programs were used.

Time-of-flight neutron powder diffraction data were collected at room temperature using the POLARIS diffractometer at the ISIS Facility, U.K. The backscattering detector bank which covers the scattering angles 130 < 2θ < 160 was used, providing data over the d spacing range 0.2 < d (Å) < 3.2 with a resolution of $\Delta d/d = 5 \times 10^{-3}$. The normalized diffraction data were corrected for absorption and Rietveld analysis was carried out using values of neutron scattering length from GSAS library (b_{Nd} = 7.69 fm, b_{Ba} = 5.25 fm, b_{Cu} = 7.72 fm, b_O = 5.81 fm). The other experimental details are presented in Table 1.

Scanning electron microscopy (SEM) and energy-dispersive spectroscopy (EDS) investigations were carried out by Hitachi field emission SEM MODEL S-4500 equipped with an EDS detector and the QUASAR-Kevex Software for Quantitative X-ray microanalysis. For calibration of EDS we used dense samples of $Nd_4Ba_2Cu_2O_{10}$, while the systematic error was estimated by analysis of $BaCuO_2$ and Nd_2CuO_4 samples.

Electron diffraction patterns were obtained by JEOL-200EX TEM, operated at 200 kV using a double-tilt holder. The sample was thoroughly ground in absolute methanol. After the sedimentation of heavy particles, a drop of liquid was placed onto the Cu grid covered by holey carbon film and left under ambient conditions until all methanol was evaporated.

Raman scattering data were taken by means of Jobin Yvon/Atago Bussan T64000 Raman triple spectrometer in macro configuration with the laser spot ≈ 100 μm. For excitation, a wavelength of 514.5 nm of a Ar^+ laser with laser power = 100 mW was used. Raman spectra were collected in backscattering geometry by using a liquid nitrogen-cooled CCD detector at room temperature in the air. IR spectrum was recorded by a SYSTEM 2000 FT-IR Perkin-Elmer spectrometer using polyethylene as dilutant.

Table 1. Unit Cell Parameters of $Nd_{1.9}Ba_{1.1}Cu_3O_{7.28}$ and Experimental Conditions of XRD and TOF Data Collection

	XRD	TOF
space group	*Ammm* (no. 65)	
a (Å)	3.8565(1)	
b (Å)	7.7724(3)	
c (Å)	22.9862(8)	
V (Å^3)	689.00(6)	
Z	4	
D_{calc} (g/cm^3)	7.058	
pattern range		
2θ (deg)	20−120	-
d (Å)	4.434−0.890	3.0−0.324
no. of reflections	347	7942
no. of parameters[a]	77	
R_{wp}[b]	0.0493	0.0183
R_p[b]	0.0379	0.0359
R_B[c]	0.0462	0.0270
R_F[c]	0.0403	0.0270
χ^2 [b]	2.697	11.06

[a] For CuO and Nd_2CuO_4 only phase fraction coefficients were refined independently. [b] For refinement of crystal structure using joint XRD and TOF data sets R_{wp} = 0.0233, R_p = 0.0379, and χ^2 = 4.885. [c] $R_B = \sum(|F_o|^2 - |F_c|^2)/\sum(|F_o|^2)$; $R_F = \sum(|F_o| - |F_c|)/\sum(|F_o|)$.

Results

Sample Characterization. According to the XRD both samples with x = 0.9 and 0.95 contained $Nd_{1+x}Ba_{2-x}Cu_3O_z$ as a major phase and a small amount of impurity−CuO. The intensity of the strongest peak of copper oxide was less than 2%. Additional examination of the samples by SEM with EDS revealed a small amount of another impurity phase−Nd_2CuO_4, which was also detected on the TOF pattern. The chemical composition of $Nd_{1+x}Ba_{2-x}Cu_3O_z$ grains was estimated to be Nd:Ba:Cu = 1.91(4):1.05(5):3.04(5). The amount of Cu^{3+} determined by iodometric titration corresponds to the oxygen content of z = 7.28(2) for both samples. In the discussion part we will focus on the studies of $Nd_{1.9}Ba_{1.1}Cu_3O_{7.28}$ composition; however, we did not observe a significant difference between lattice constants, Raman or IR spectra of both solid solutions.

The reflections from superstructure on the XRD pattern were quite weak and relative intensity did not exceed 3%. In the case of time-of-flight neutron diffraction data, the relative reflection intensities from superstructure reached 10%.

Raman and IR Spectroscopy. Raman and IR spectra of $Nd_{1.9}Ba_{1.1}Cu_3O_{7.28}$ are presented in Figure 1.

(16) Kakihana, M. J. *Sol−Gel Sci. Technol.* **1996**, *6*, 7.
(17) Larson, A. C.; Von Dreele, R. B. Los Alamos Laboratory Report No LA-UR-86-748, 1987.
(18) (a) Sheldrick, G. M. *SHELXS-97 − A program for automatic solution of crystal structures*; University of Goettingen: Goettingen, Germany, 1997; Release 97-2. (b) Sheldrick, G. M. *Acta Crystallogr. A* **1990**, *46*, 467.

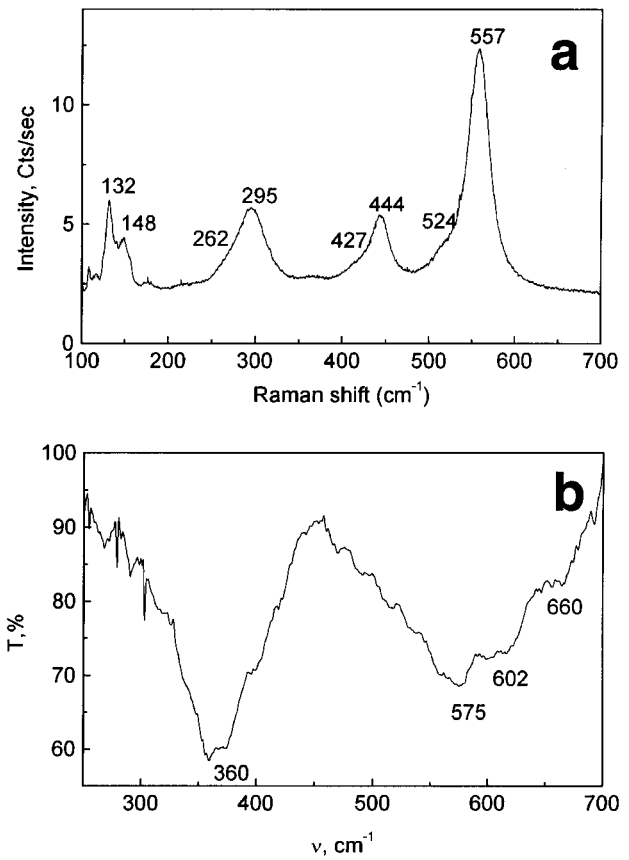

Figure 1. (a) Macro-Raman spectrum of $Nd_{1.9}Ba_{1.1}Cu_3O_{7.28}$ and (b) FT-IR spectrum of $Nd_{1.9}Ba_{1.1}Cu_3O_{7.28}$.

One can see that phonons are only active either in Raman (Figure 1a) or IR spectrum (Figure 1b). There is no band that is present in both spectra. Examination of the character tables[19] help conclude that this is possible only for orthorhombic space groups that possess an inversion center. It should be mentioned that the IR-active mode at 602 cm^{-1} which is assigned to vibrations of oxygen atoms in the Cu−O chains[20] is absent or too weak to be observed in the Raman spectrum of $Nd_{1.9}Ba_{1.1}Cu_3O_{7.28}$ despite the fact that the oxygen content is higher than 7. Addition of an extra oxygen atom to the chain site of ideal $NdBa_2Cu_3O_7$ structure would result in the removal of the translation invariance and appearance of this band as a defect-induced Raman mode. Absence of this vibration in the Raman spectrum indicates ordering of the extra chain oxygen in the supercell of $Nd_2BaCu_3O_z$. The observation of extra mode at 575 cm^{-1} in Raman spectra of rapidly quenched samples,[21] which disappeared upon oxygenation, supports the idea about oxygen ordering in the supercell and presence of inversion center.

TEM and Electron Diffraction. Electron diffraction patterns from samples with the chemical composition of $Nd_{1.9}Ba_{1.1}Cu_3O_{7.28}$ with the electron beam incident along [100], [010], and [001] directions are presented in Figure 2 a−c. One can see that *b* and *c* axis of the lattice are doubled compared to normal $NdBa_2Cu_3O_7$ structure and lattice parameters are $a = 3.8$ Å, $b = 7.7$ Å, and $c = 22.9$ Å. The striking difference with the previous investigation[6] is that there is no special limiting reflection condition and it allows choosing *Pmmm* space group for the possible structural model. More detailed investigation by TEM revealed twinning present in the particles of $Nd_2BaCu_3O_z$ (Figure 3a), which was the main difficulty for the preparation of single crystals for X-ray structure investigation.[22] In the case of $YBa_2Cu_3O_7$, the twin structure appears as the result of $P4/mmm \rightarrow Pmmm$ phase transformation, which takes place during oxidation of this compound. $Nd_2BaCu_3O_z$ is known to have orthorhombic cell even at high temperature[22] and the observed twins must be due to another orthorhombic-to-tetragonal phase transformation which probably occurs during the diffusion of Nd ions into $Nd_{1+x}Ba_{2-x}Cu_3O_z$ solid solution with the tetragonal lattice. In fact, during the intermediate

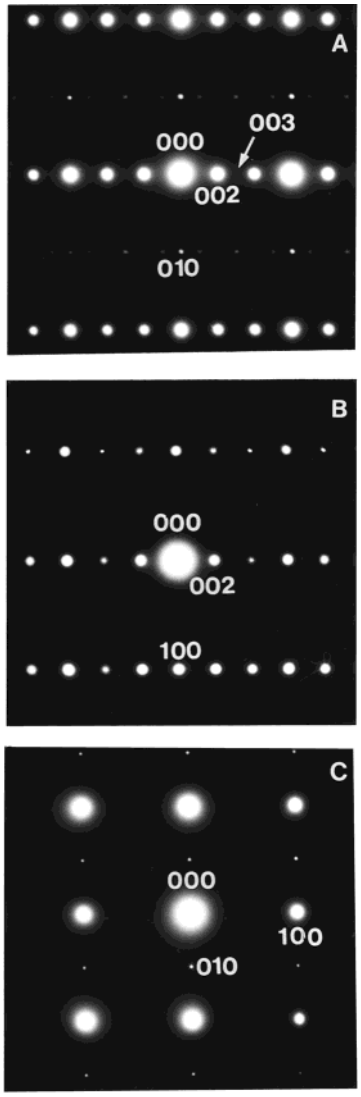

Figure 2. SAED patterns of the $Nd_{1.9}Ba_{1.1}Cu_3O_{7.28}$ taken at 200 kV and 80 cm camera length: (a) electron beam incident along [100] direction, (b) electron beam incident along [010] direction, and (c) electron beam incident along [001] direction.

(19) Cotton, F. A. *Chemical Applications of Group Theory*, 3rd ed.; John Willey & Sons: New York, 1990.
(20) Ivanov, V. G.; Iliev, M. N. *Physica C* **1995**, *244*, 293.
(21) Goodilin, E.; Limonov, M.; Panfilov, A.; Khasanova, N.; Oka, A.; Tajima, S.; Shiohara, Y. *Physica C* **1998**, *300*, 250.
(22) Goodilin, E.; Oka, A.; Wen, J. G.; Shiohara, Y.; Kambara, M.; Umeda, T. *Physica C* **1998**, *299*, 279.

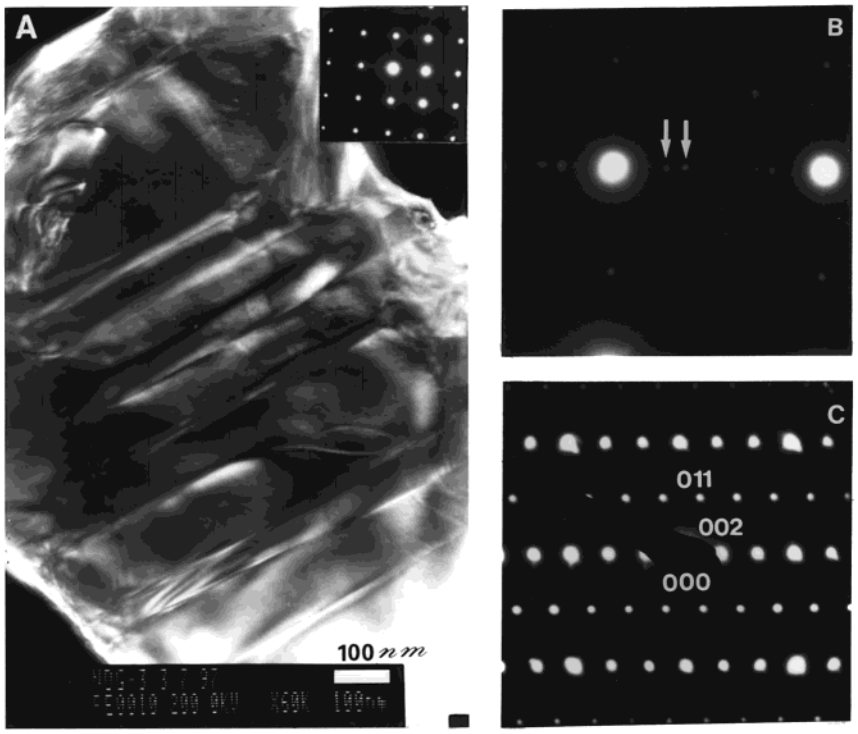

Figure 3. (a) particle of $Nd_{1.9}Ba_{1.1}Cu_3O_{7.28}$, beam incidence along [001] direction, (magnification 60K), (b) electron diffraction with the beam incidence along [001] (distance between superstructural reflections corresponds to 45−48 Å); (c) electron diffraction pattern with the beam incidence along [100] with the systematic absence of $k + l = 2n + 1$ reflections.

grindings we observed Nd_2CuO_4 as a main impurity on the X-ray diffraction patterns and it means that intermediate composition was Nd-deficient compared to the final compound. Another interesting feature, that is quite rare, is the diffraction from the superlattice with the large period about 45−48 Å shown in Figure 3b. Probably it reflects the more complicated oxygen ordering that is possible in $Nd_2BaCu_3O_z$ and it was not taken into account during the structure solution and refinement. In the few cases we also observed diffraction pattern for [100] incident beam similar to the previously reported[6] with the systematic absence of $k + l = 2n + 1$ reflections (Figure 3c). However we initially choose the *Pmmm* space group for the structure solution in accordance with frequently observed ED patterns.

X-ray and Neutron Powder Diffraction Data. *Structure Solution and Refinement.* The first approximation of the lattice parameters was made by the least-squares method using XRD data collected with the Si as internal standard. One atom (Cu at (0,0,0)) was introduced into the structural model. One atom is required by GSAS[17] to extract intensities by Le Bail method.[23] The occupation factor of this atom was set to zero, two regions with the strongest peaks of CuO were excluded from histogram, and intensities of 681 reflections were extracted.

In the instructions file for SHELXS, we indicated ideal composition $Nd_8Ba_4Cu_{12}O_{29}$ of the elementary unit cell. However the program located 12 unique heavy atoms positions ($R = 0.38$) corresponding to the unit cell content $Nd_4Ba_8Cu_{18}$. While Nd/Ba atoms and the first four Cu atoms multiplied by symmetry operations formed slightly distorted skeleton similar to common $NdBa_2Cu_3O_7$ structure doubled along *b* and *c* axes and shifted from the origin of the space group along (120), the other found Cu atoms laid in the positions normally occupied by chain and in-plane oxygen with the corresponding "Cu−Cu" distance about 1.9 Å. The failure to distinguish Cu and lighter atoms probably occurred because of the small number of reflections used for structure solution by direct method or by error of the intensity estimation of overlapped reflections. It was decided to use only the first four located copper atoms for the next step and Nd/Ba positions were kept statistically occupied by Nd and Ba.

Structure Refinement by Rietveld Method. The experimental details of XRD and TOF data collection as well as results of structure refinement are summarized in Table 1. At first, positions of heavy atoms were refined by the Rietveld method using the X-ray powder diffraction data. Upon the refinement of the cation framework, oxygen atoms were located from difference Fourier synthesis map. After this step, we continued structure determination using XRD and TOF powder data sets simultaneously. The advantage of such an approach is that it allows avoiding false minima, distinguishing Ba and Nd atoms that have close X-ray scattering factors and locating oxygen atoms more precisely.

At the final stage of the refinement the thermal parameters of two Nd/Ba atoms at (0,0,0.0846) and $(0,{}^1/_2,0.4166)$ (Table 2) tended to be large—$\sim$8.1 Å^2, while for the other Nd/Ba sites thermal parameters were close to zero and even slightly negative at $z \approx 0.25$. On the other hand the interatomic distances Nd/Ba−O from the atoms with large thermal parameters to the oxygen atoms in the nearest coordination were 2.72−

(23) Le Bail, A.; Duroi, H.; Fourquet, J. L. *Mater. Res. Bull* **1988**, *23*, 447.

Table 2. Refined Atomic Positions, Thermal Parameters, and Occupancies for $Nd_{1.9}Ba_{1.1}Cu_3O_{7.28}$[a]

atom	*x*	*y*	*z*	occupancy
Ba(1)	0	0	0.08446(8)	1
Nd(1)	0	0	0.24712(6)	1
Nd(2)	0	0	0.40428(6)	0.9
Ba(2)	0	0	0.40428(6)	0.1
Cu(1)	1/2	0.28241(15)	0	1
Cu(2)	1/2	0.25024(16)	0.17474(3)	1
O(1)	0	0.3076(6)	0	0.56(1)
O(2)	1/2	0.29528(17)	0.08032(5)	1
O(3)	0	0.2565(2)	0.18328(7)	1
O(4)	1/2	0	0.18187(12)	1
O(5)	1/2	0	0.31439(11)	1
O(6)	1/2	0	0	1.03(2)

atom	U_{11}	U_{22}	U_{33}	U_{12}	U_{13}	U_{23}
Ba(1)	0.0113(9)	0.0205(9)	0.0095(8)	0	0	0
Nd(1)	0.0024(4)	0.0029(5)	0.00205(32)	0	0	0
Nd(2)	0.0056(7)	0.0040(6)	0.01808(63)	0	0	0
Ba(2)	0.0056(7)	0.0040(6)	0.01808(63)	0	0	0
Cu(1)	0.02836(82)	0.0096(6)	0.00284(35)	0	0	0
Cu(2)	0.00266(22)	0.00407(25)	0.00746(26)	0	0	0.00161(32)
O(1)	0.0123(18)	0.0320(23)	0.0100(15)	0	0	0
O(2)	0.0261(8)	0.0181(6)	0.0042(4)	0	0	−0.0002(5)
O(3)	0.00200(33)	0.0068(4)	0.0138(9)	0	0	−0.0029(5)
O(4)	0.01156(89)	0.0045(7)	0.0067(10)	0	0	0
O(5)	0.00331(67)	0.0017(6)	0.0133(10)	0	0	0
O(6)	0.0081(19)	0.1848(65)	0.00173(24)	0	0	0

[a] *T*-thermal correction:[17] $T = \exp[-2\pi^2(U_{11}h^2a^{*2} + ... + 2U_{12}hka^*b^* + ...)]$.

3.03 Å which is larger than the other Nd/Ba−O distances in this compound 2.45−2.70 Å and closer to Ba−O distance in $NdBa_2Cu_3O_7$ 2.71 Å and 2.92 Å rather than to Nd−O bond length in $Nd_{1+x}Ba_{2-x}Cu_3O_z$ solid solutions 2.47 Å.[9,12] The latter fact probably indicates the preferential occupation of these particular sites by Ba atoms (calculated valence[24] was 2.16 for Ba and 1.33 for Nd), while the rest of Nd/Ba sites are occupied by Nd atoms (calculated valence for Nd was 2.6−2.7 and for Ba, 3.7−4.4). Such a conclusion explains well high thermal parameters of the atoms resulted from our initial assumption about the statistical occupation of all Nd/Ba sites. This was taken into account in the further refinement.

Upon refinement it was found that all but chain oxygen atoms form a unit cell of higher symmetry namely *Ammm* within 0.1 Å. More detailed investigation of X-ray and TOF diffraction patterns reveled that only few very weak reflections do not agree with the $k + l = 2n + 1$ limiting condition. This explains well appearance of $k + l = 2n + 1$ reflection condition on the ED patterns (Figure 3c). Probably frequently observed ED pattern shown on the Figure 2a corresponds to the conjugated domains with [100] and [001] orientation toward the incident beam. Although the reflection 010 present in Figure 2c is not allowed for *Ammm* space group, the structure should probably be considered as a face-centered to explain the limiting conditions on the Figure 2b and, in addition this reflection was never observed in the related compounds, e.g. $YNdBaCu_3O_z$.

At the last step the structure was refined within *Ammm* space group, we applied constraints for the total oxygen content to be equal to the value 7.28(2) determined by iodometric titration and refined thermal parameters and occupation of the oxygen sites. The results of the structure refinement are summarized in Table 2. Table 3 gives selected interatomic distances, Figure 4 shows XRD and TOF data with the results of structure refinement by Rietveld method. Detailed investigation of the difference Fourier maps did not reveal any extra atoms.

(24) Brown, I. D.; Altermatt, D. *Acta Crystallogr. B* **1985**, *41*, 244.

Table 3. Selected Interatomic Distances for $Nd_{1.9}Ba_{1.1}Cu_3O_{7.28}$[a]

bond	no. of bonds	*d* (Å)	bond	no. of bonds	*d* (Å)
Ba(1)−O(1)	2	3.080(4)	Cu(1)−O(1)	2	1.9382(5)
Ba(1)−O(2)	4	2.9991(10)	Cu(1)−O(2)	2	1.8490(11)
Ba(1)−O(3)	2	3.0226(21)	Cu(1)−O(6)	1	2.1950(12)
Ba(1)−O(4)	2	2.9549(25)			
Ba(1)−O(6)	2	2.7363(13)	Cu(2)−O(2)	1	2.1984(11)
Cu(2)−O(3)	2	1.93885(20)			
Nd(1)−O(3)	2	2.4760(17)	Cu(2)−O(4)	1	1.9519(13)
Nd(1)−O(3′	2	2.4777(17)	Cu(2)−O(5)	1	1.9572(13)
Nd(1)−O(4)	2	2.4430(20)			
Nd(1)−O(5)	2	2.4717(20)			
Nd(2)/Ba(2)−O(1)	2	2.6601(29)			
Nd(2)/Ba(2)−O(2)	4	2.5249(9)			
Nd(2)/Ba(2)−O(3)	2	2.7624(18)			
Nd(2)/Ba(2)−O(5)	2	2.8262(22)			

[a] Calculated valences:[24] V(Ba(1)) = 2.004; V(Nd(1)) = 3.009; V(Nd(2)) = 2.355; V(Ba(2)) = 3.831; V(Cu(1)) = 2.504; V(Cu(2)) = 2.186.

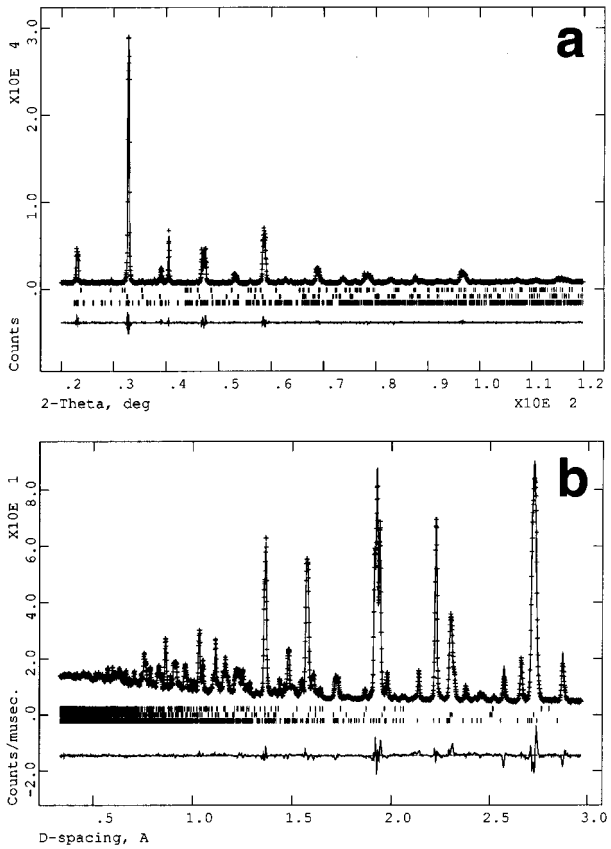

Figure 4. (a) Experimantal (hatched line), calculated (solid line), and difference (bottom) powder X-ray diffraction profiles for the Rietveld refinement of $Nd_{1.9}Ba_{1.1}Cu_3O_{7.28}$ crystal structure and (b) experimantal (hatched line), calculated (solid line), and difference (bottom) powder TOF profiles for the Rietveld refinement of $Nd_{1.9}Ba_{1.1}Cu_3O_{7.28}$ crystal structure.

Discussions

Crystal Structure of $Nd_{1.9}Ba_{1.1}Cu_3O_{7.28}$. The determined structure of the elementary unit cell is dis-

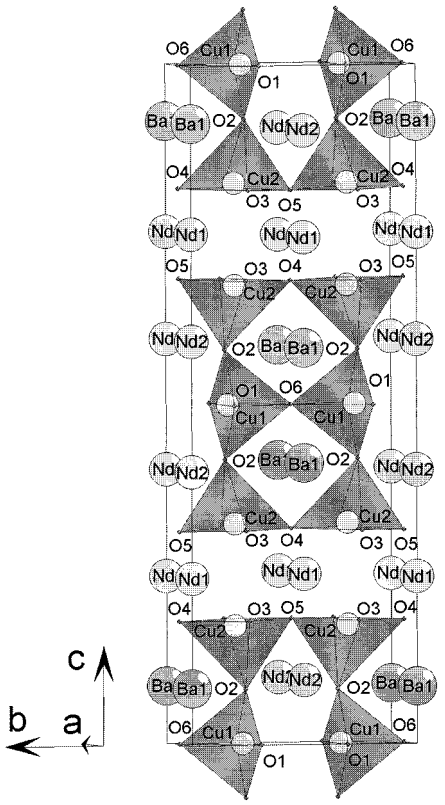

Figure 5. Crystal structure of $Nd_{1.9}Ba_{1.1}Cu_3O_{7.28}$ refined from XRD and TOF powder data.

played in Figure 5. Crystal structure of $Nd_2BaCu_3O_z$ can be derived from the structure of $NdBa_2Cu_3O_7$ by doubling the unit cell along *b* and *c* axes and by ordering Nd and Ba atoms in the Ba site. The heavy atoms form a face-centered lattice. It should be noted that the way of Nd and Ba arrangement as well as location of oxygen atoms is significantly different from the initially proposed structure[6] determined from X-ray powder diffraction with *B*2*mm* symmetry. However one may expect lower unit cell symmetry for the oxygen deficient $Nd_2BaCu_3O_z$ due to the disorder in the Cu(1)−O(1)−O(6) plane similar to $YBa_2Cu_3O_z$ case.

It is important that excess oxygen atoms occupy vacant position near Ba atoms while vacant position near Nd atom between Cu−O chains remains empty (Figure 5). The most ambiguous result of structure refinement is high oxygen thermal parameters in the CuO plane at $z = 0$. Examination of the δF map of this plane shows that additional scattering density is present at ($^1/_2$,±*y*,0). First, it was assumed that Cu atom in this plane could be partially replaced by carbon, which may lead to the distortions in the considered site due to the short C−O fragment, but we observed internal modes of CO_3^{2-} group neither in Raman nor in IR spectra. In addition bond distance between Cu(1) and displaced oxygen O(6) 1.86 Å is rather large for C−O bond. This bond length is close to the Cu(1)−O(2) distance and leads to think that Cu(1) could be four coordinated due to the deviation of crystal structure from ideal one. In the later case additional oxygen atom enters ($^1/_2$,$^1/_2$,0) site, while O(1) is removed. O(6) shifts from the ideal position and new defect fragment forms as it is shown in Figure 6. Incorporation of additional oxygen into

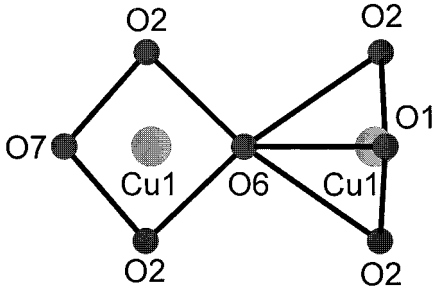

Figure 6. Possible local oxygen arrangement in the vicinity of Cu(1) atoms.

($^1/_2$,$^1/_2$,0) indicates that Ba(2) is not randomly scattered in the crystal but forms clusters which allow oxygen to occupy vacant sites and decrease strain in the adjacent CuO_5 pyramids (Figure 6). Probably long-range ordering of such defects is responsible for the extra reflections in Figure 3b. One may also assume existence of vacancy on the Nd(2) site, since the calculated Ba(2) valence is quite high (Table 3). Such a possibility can be neither proved nor rejected on the basis of the available data due to the high correlation between thermal parameter and occupancy and small possible deviation from the stoichiometry. However it should be noted that such defects are not common in the case of high-T_c superconductors, which possess similar structural blocks.

Usually positions of extra oxygen atoms are not widely discussed for the case of $Nd_{1+x}Ba_{2-x}Cu_3O_z$ solid solutions, and it is implied that extra charge of Nd^{3+} in the place of Ba^{2+} atom must be compensated due to the attraction of the additional oxygen ion in the nearest coordination. Nevertheless, the structure of $Nd_2BaCu_3O_z$ clearly demonstrates that it is not the case. This fact should be taken into account for the speculations about mechanisms of superconductivity suppression in the case of $Ln_{1+x}Ba_{2-x}Cu_3O_z$ (Ln—lanthanide) solid solutions. The described type of the Nd−Ba and oxygen ordering may provide an ideal periodically distributed pinning centers in the superconducting solid solutions being responsible for the anomalous j_c vs H dependence in this class of materials.

Symmetry Analysis. Group theoretical analysis for the determined structure using the nuclear site group approach[25] gives an irreducible representation of the lattice modes in the form:

$$\Gamma = 13A_g + 3A_u + 13B_{1g} + 11B_{1u} + 8B_{2g} + 14B_{2u} + 5B_{3g} + 14B_{3u}$$

where vibrations of extra oxygen atom O(6) must contribute to B_{1u}, B_{2u}, and B_{3u} phonons inactive in Raman spectrum. This is in a good agreement with the experimental Raman and IR data (Figure 1) and explains absence of disorder-induced peaks for $Nd_{1+x}Ba_{2-x}Cu_3O_z$ solid solutions with high *x* when *z* becomes larger than 7.00. Nevertheless, it should be mentioned that chain-site oxygen atom O(1) is not in the origin of the space group any longer and their vibrations must be observed in Raman spectrum since the reducible representation of corresponding phonons contains A_g, B_{1g}, and B_{3g}

(25) Rousseau, D. L.; Bauman, R. P.; Porto, S. P. S. *J. Raman Spectrosc.* **1981**, *10*, 253.

irreducible representations. To understand this phenomenon, quantitative estimation of lattice vibration frequencies is required.

Acknowledgment. We are thankful to Professor E. V. Antipov (Moscow State University) for useful comments on this work and to Dr. M. Gülgün (MPI-Stuttgart) for discussions of TEM-ED results. One of us V.V.P. is grateful to the Ministry of Culture and Education of Japan (Monbusho) for providing him the scholarship in 1998.

Supporting Information Available: Structure factors for X-ray diffraction data. This material is available free of charge via the Internet at http://pubs.acs.org.

CM990021W